G. Zucca et alii, Frattura ed Integrità Strutturale, 30 (2014) 409-416; DOI: 10.3221/IGF-ESIS.30.49

Focussed on: Fracture and Structural Integrity related Issues

Failure of cargo aileron's actuator

G. Zucca, M. Amura, L. Allegrucci, M. Bernabei

Italian Air Force, Flight Test Centre, Chemistry Department, Military Airport M. De Bernardi, via Pratica di Mare, Pomezia (RM), 00040, Italy

guido.zucca@aeronautica.difesa.it, mikael.amura@aeronautica.difesa.it, laura.allegrucci@aeronautica.difesa.it, manuele.bernabei@aeronautica.difesa.it

ABSTRACT. During a ferry flight, in a standard operation condition and at cruising level, a military cargo experienced a double hydraulic system failure due to a structural damage of the dual booster actuator. The booster actuator is the main component in mechanism of aileron's deflection. The crew was able to arrange an emergency landing thanks to the spare oil onboard: load specialists refilled the hydraulic reservoirs. Due to safety concerns and in order to prevent the possibility of other similar incidents, a technical investigation took place. The study aimed to carry out the analysis of root causes of the actuator failure. The Booster actuator is composed mainly by the piston rod and its aluminum external case (AA7049). The assembly has two bronze caps on both ends. These are fixed in position by means of two retainers. At one end of the actuator case is placed a trunnion: a cylindrical protrusion used as a pivoting point on the aircraft. The fracture was located at one end of the case, on the trunnion side, in correspondence to the cap and over the retainer. One of the two fracture surfaces was found separated to the case and with the cap entangled inside. The fracture surfaces of the external case indicated fatigue crack growth followed by ductile separation. The failure analysis was performed by means of optical, metallographic, digital and electronic microscopy. The collected evidences showed a multiple initiation fracture mechanism. Moreover, 3D scanner reconstruction and numerical simulation demonstrated that dimensional non conformances and thermal loads caused an abnormal stress concentration. Stress concentration was located along the case assy outer surface where the fatigue crack originated. The progressive rupture mechanism grew under cyclical axial load due to the normal operations. Recommendations were issued in order to improve dimensional controls and assembly procedures during production and overhaul activities.

KEYWORDS. Ailerons actuator; AA7049; Multiple initiation sites fatigue; Thermal load; Dimensional non conformances.

INTRODUCTION

A military cargo airplane during a ferry flight in standard operation conditions, experienced a double failure of both the hydraulic systems on board. As a consequence, the pressure of the servo-actuators relevant to the flight controls suddenly dropped. Although the cloche became stiff, the well trained crew managed to land safely by using the spare hydraulic fluid on board to refill the reservoirs.

The subsequent inspection highlighted a rupture on the Dual Booster Actuator (DBA).

This component function is the ailerons deflection. Being a primary importance actuator for the aircraft controllability, it is connected to both the hydraulic systems for safety reasons. The main parts of the DBA are the piston rod and the external case. Two bronze caps are placed at both ends, and they are fixed in position by means of two retainers. The DBA is hinged to the aircraft by a cylindrical support fixed at one end of the actuator case, named trunnion. The fracture surface was located at the actuator case end on the trunnion side, over the retainer (Fig. 1).
This paper illustrates the failure analysis of the aforementioned actuator.

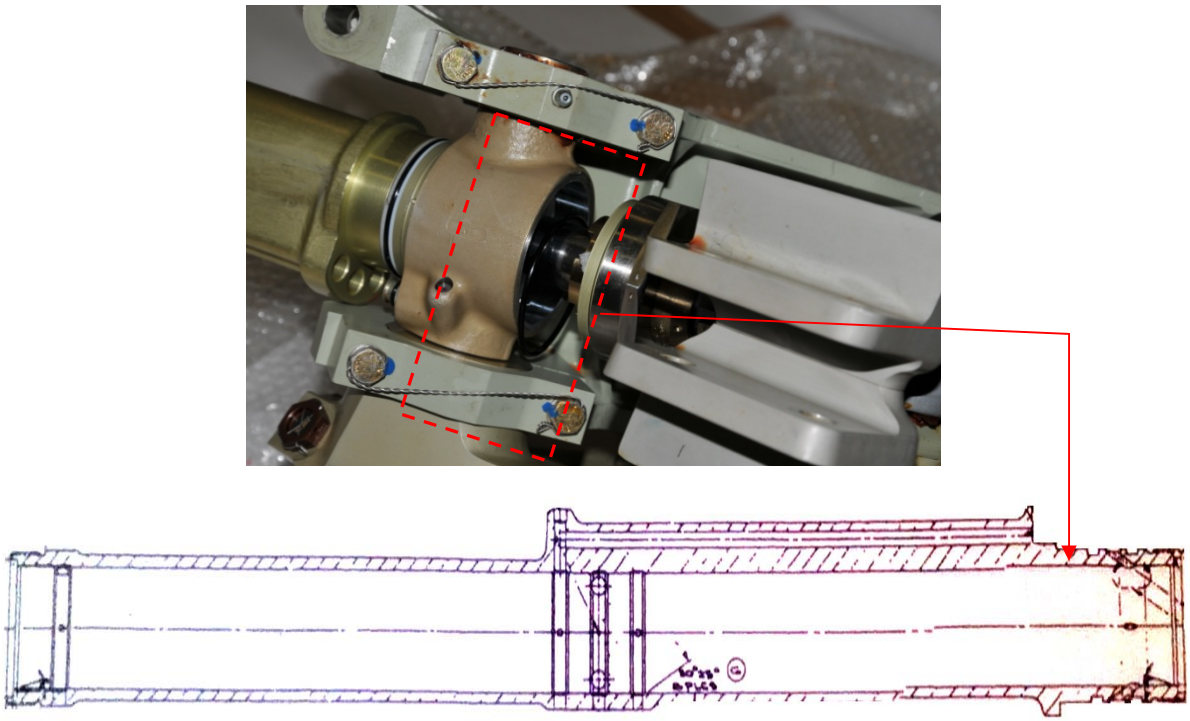

Figure 1: Rupture position.

INSTRUMENTS

Optical examination was carried out using a Leica M 205 C microscope. Microfractographical evidences were acquired by a Gemini Ultra Plus Field Emission Scanning Electron Microscope (FESEM) equipped with an INCAx-Sight Oxford Instruments Xray energy dispersive spectroscopy (EDS) to perform a semi-quantitative microanalysis exam. Microstructural examination was made using a Leica CTR 6000 metallographic microscope, whereas a PANalytical Axios Max to perform X-ray Fluorescence Spectroscopy was used to determine the chemical composition of the forging. Hardness measurements were carried out with A200 Hardness Rockwell Tester Officine Galileo and Leica VMHT Auto. Metrologic measurements were performed using Konica Minolta RANGE 7 3D scanner. FEA was carried out by ANSYS 14.0 software program.

RESULTS

Visual and Optical observation.

The cap was found entangled inside the detached fracture surface and some force was needed to remove it (Fig. 2). However, no damages were produced in this operation. The two fracture surfaces showed the same features. The fracture started from the external surface, and propagated toward the internal one. The fracture surface was divided in two zones, named A and B (Fig. 3). Zone A was rough, dull, characterized by coarse grains and it was oriented at about 45° to the transversal section. Moreover, a plastic deformation, associated to the final phase of the failure, was

observed. Therefore, Zone A was the region of the final, unstable fracture. Zone B was characterized by a fracture surface flat, smooth and bright with beach marks typical of fatigue crack growth. (Fig. 4). On the external surface's edge there were ratchet marks, showed by black arrows in Fig. 4. However, also in the 45° orientation areas, there was a small flat area running all around on the external side (black arrow in Fig. 5) showing ratchet marks.

Figure 2: Cap entangled inside the fracture surface.

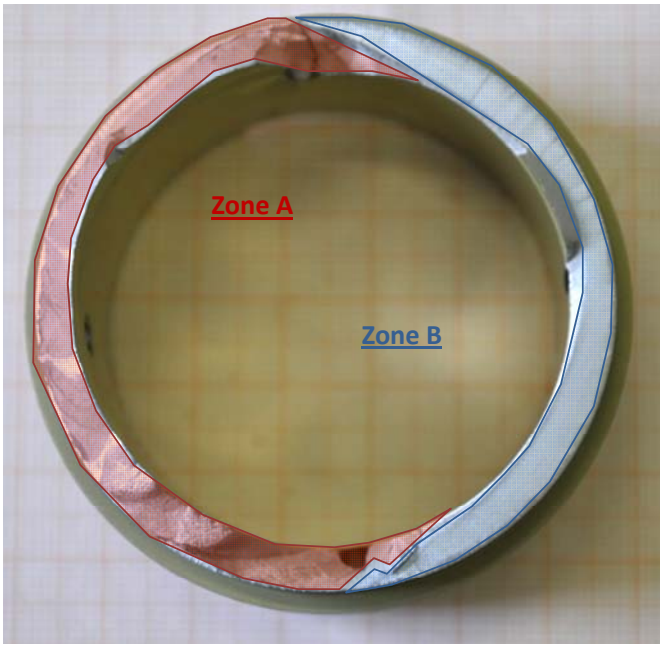

Figure 3: Fracture surface.

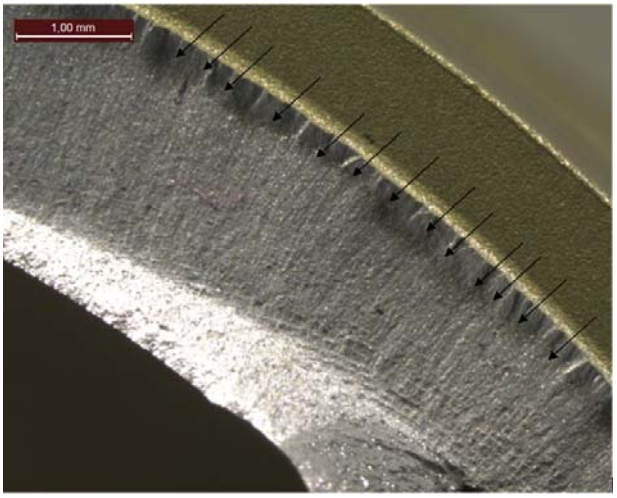

Figure 4: Beach marks and ratchet marks on the surface's edge.

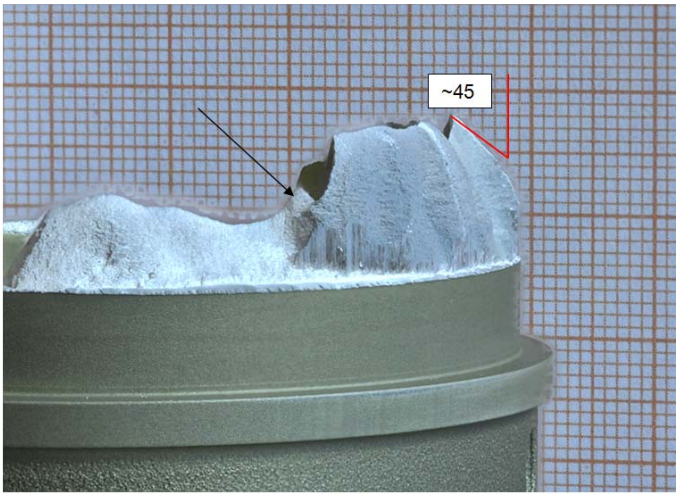

Figure 5: Fracture detail.

Electronic Microscopy

FESEM observations of the Zone B of fracture surface confirmed the presence of the fatigue crack mechanism Fig. 6 and Fig. 7. Multiple initiation sites of the fatigue crack are all around the external edge of the fracture surface. Zone A showed dimples and microvoid, these are evidences of unstable fatigue crack propagation (Fig. 8) [1].

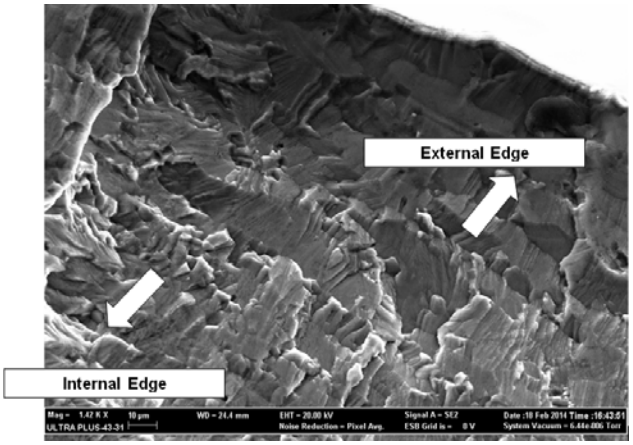

Figure 6: Area of fatigue crack propagation.

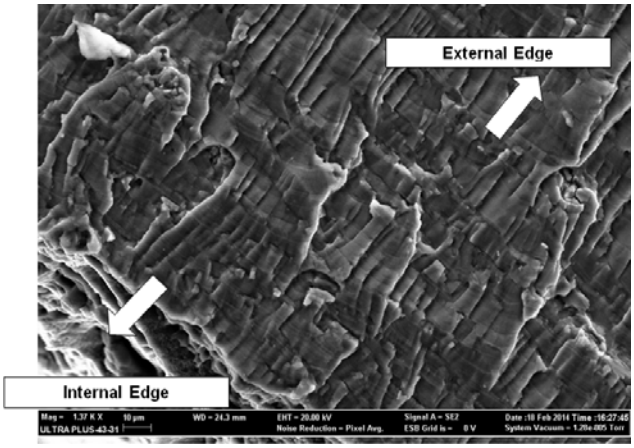

Figure 7: Area of fatigue crack propagation.

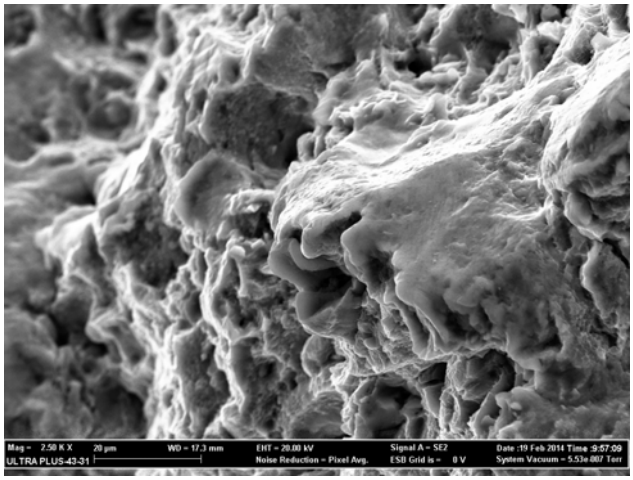

Figure 8: Dimples and microvoid.

Figure 9: Striation spacing.

In Zone B in the stable propagation phase of the fatigue phenomenon the striations spacing was about 60 nm (Fig. 9) [2] [3].

3D Reconstruction and metrologic measurement.

Actuator case and cap geometry were acquired using a 3D scanner Fig. 10 e Fig. 11, the diameters were measured in 8 points as showed in Fig. 12 e Fig. 13.

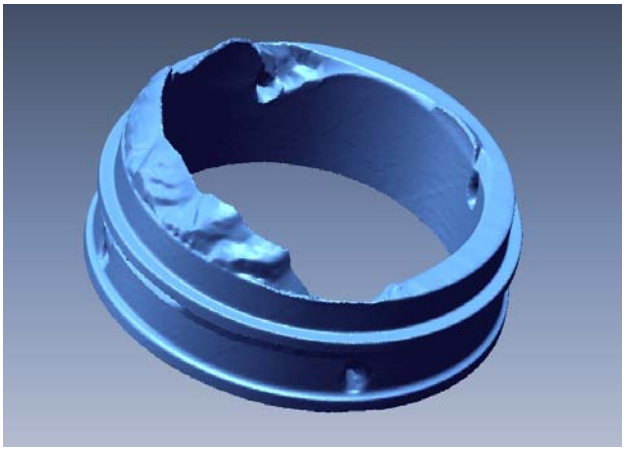

Figure 10: Actuator case, digital geometry.

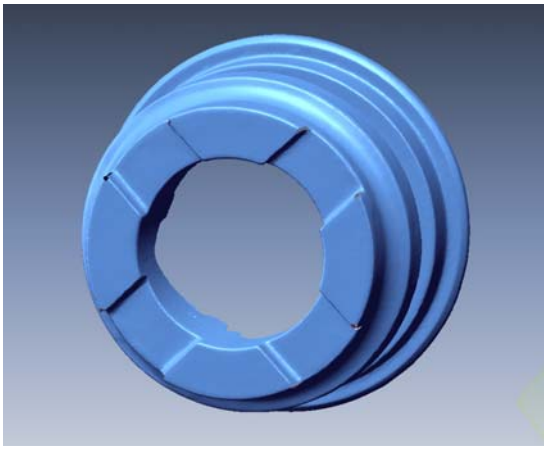

Figure 11: Cap, digital geometry.

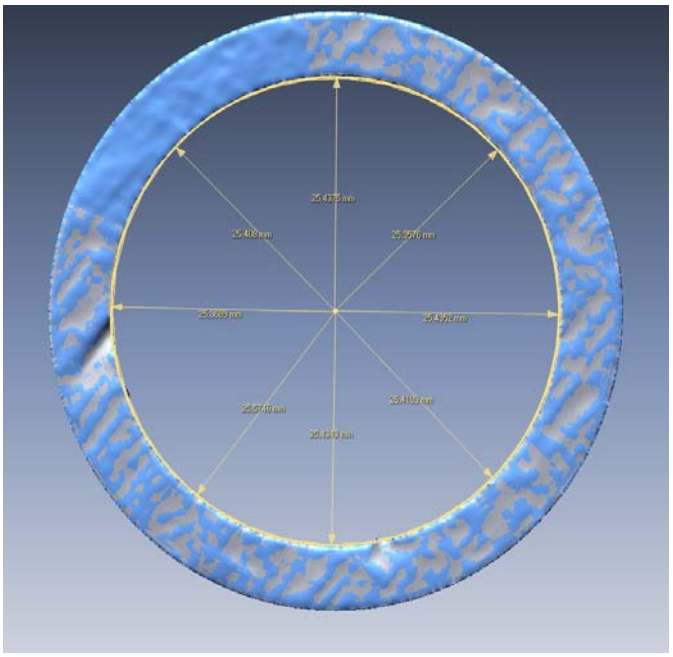

Figure 12: Actuator Case internal diameter measurements.

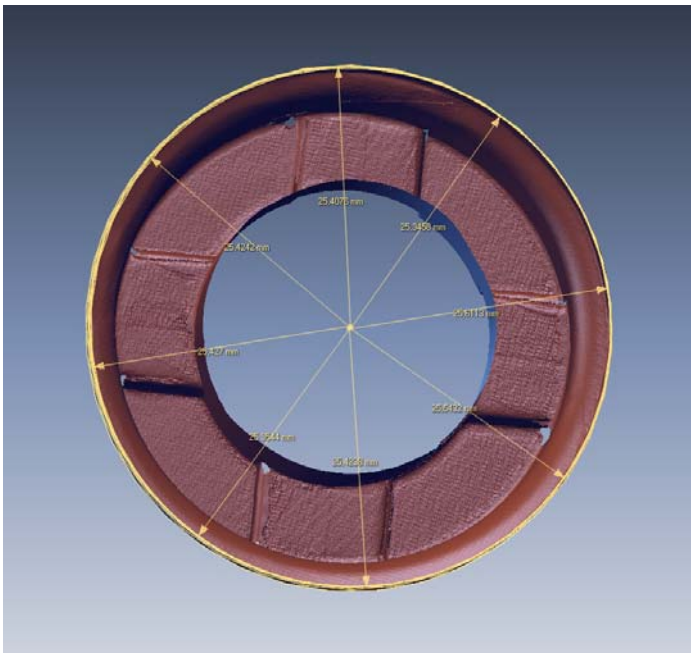

Figure 13: Cap external diameter measurements.

Results are showed in Tab. 1.

The two parts have an average mechanical interference of 25 μm. This was the reason of the tight fit observed during disassembly operations between external case and cap.

	Mean Diameter [mm]	Mean Coupling [mm]
Cap	50.8843±0.1498	-0.025
Actuator case	50.8587±0.0565	

Table 1: Results of measurement.

Design drawing values are:

Diameter of Actuator Case	2.000 – 2.002 inches (50.8000 - 50.8508 mm)
Diameter of Cap	1.998 – 1.999 inches (50.7492 - 50.7746 mm)

Table 2: Drawing requirements.

Therefore, the required gap should be comprised between 25.4 to 101.6 μm.

Microstructural analysis.

A Microstructural examination, were performed on two sections of actuator case made orthogonally and parallel to its axis. The examination, revealed the joint zone between the two halves of the actuator case, showing two different microstructures [4]. Transition is showed in Fig. 14. Hardness test will evaluate mechanical consequences of this anomaly. Another section, near the oil chamfer was analyzed, in order to evaluate the shot peening treatment required by design.

Chemical analisys and conductivity test.

X-Ray fluorescence (XRF) showed that the actuator case samples were in accordance with the specification for a 7049 [5] [6] aluminum alloy. Alloy homogeneity was confirmed by EDS mapping on the outer edge of the actuator case.

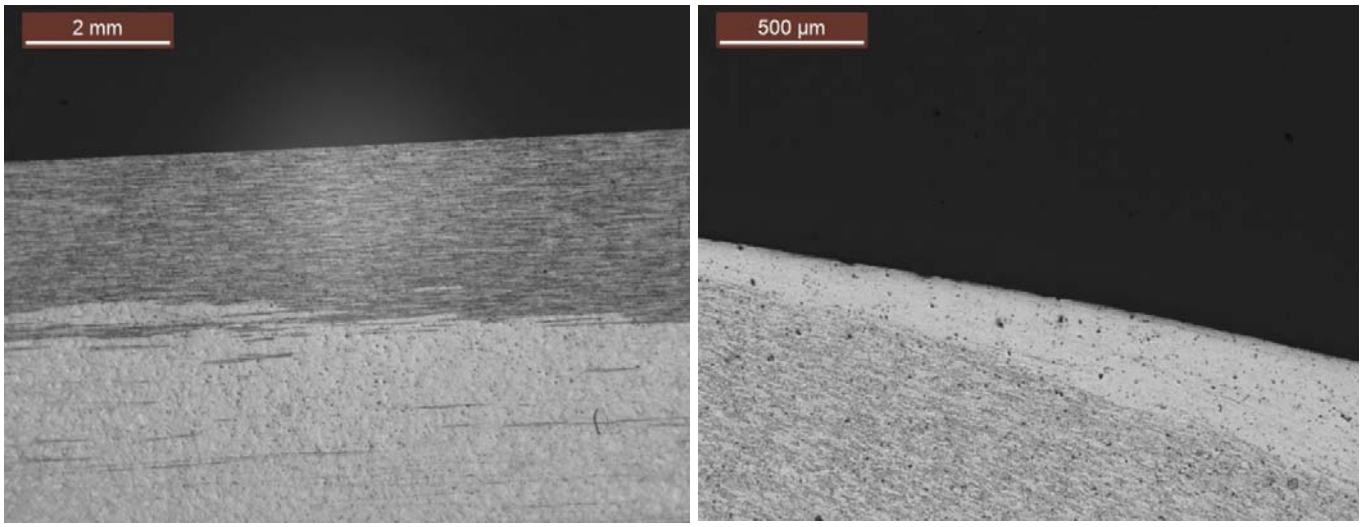

Figure 14: Transition between two halves of the actuator case.

Hardness Test

Hardness test (Tab. 3) was performed on the actuator internal and external surface in accordance to HRB. Moreover, MHV method was used across the thickness in order to evaluate the shot peening effect.

Location	Hardness	
	Mean	Std. Dev.
Internal Surface (HRB)	86.3	0.9
External Surface (HRB)	82	1.6
On the section (from outside to inside) (MHV)	175.7	3.5

Table 3: Hardness results.

The results confirm a T73 heat treatment [5] [6], while the values taken across the thickness highlight an increase in hardness where the shot peening should have been applied, confirming the correct procedure was applied during production.

Finite Element Analysis

A FEA model was performed in order to evaluate the effect of forced coupling between the actuator case and the cap. The Geometric 3D model of DBA was reproduced by the design drawings Fig. 15.

4768 hexahedrons [7] elements were applied to provide the mesh for mathematical model Fig. 15. Being impossible to reproduce exactly the geometry of the interference, it was assumed as a conservative hypothesis the perfect fit between the two parts: no gap and no interference.

The hydraulic system oil works oil within a range of 60°C - 90°C, while the pressurized cabin compartment where the DBA is placed is at about 20° C. This implies a thermal variation of $\Delta T = 40 - 70$ ° C that becomes a thermal load to the structure due to the different thermal expansion coefficient of the case assy and the cap. Indeed, the cap is made of copper alloy AMS 4631, while the case assy is AA7049. Therefore an average $\Delta T = 55$° C was applied.

Pressure and inertial loads were not simulated because no findings during the failure analysis suggested they could have been abnormal.

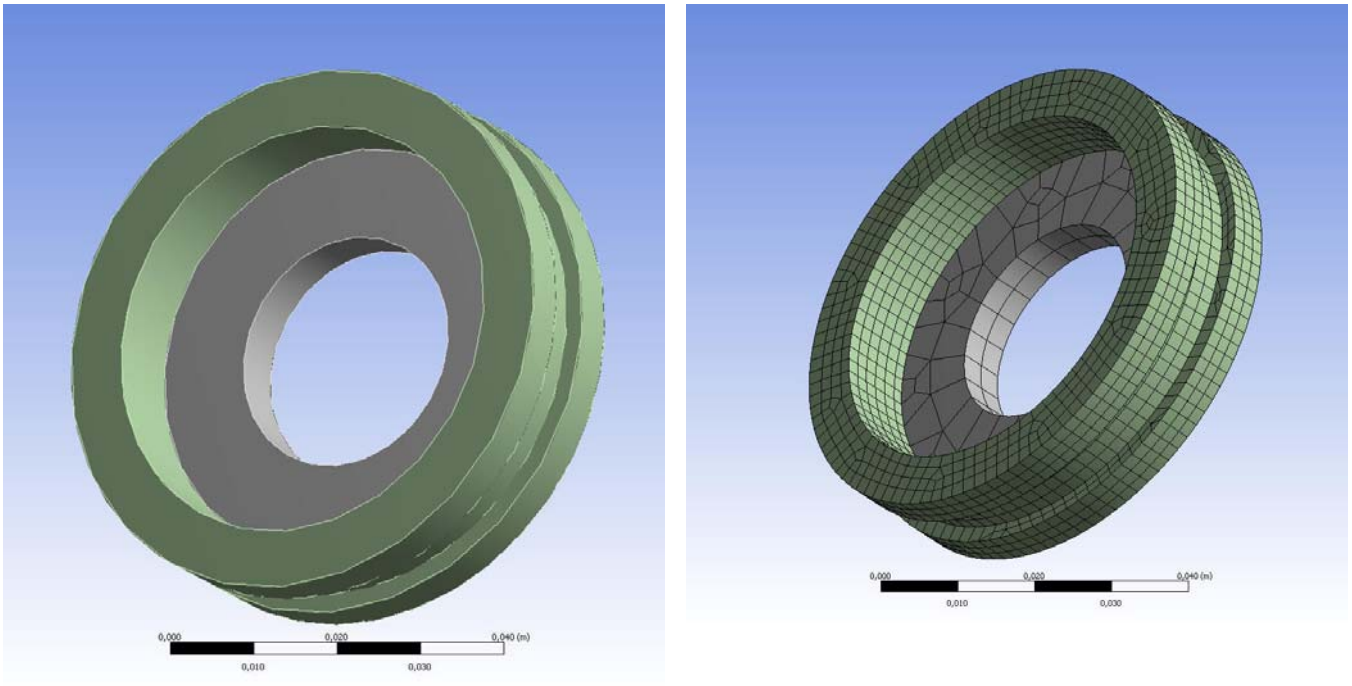

Figure 15: CAD Geometry (left), mathematical model (right).

Numerical results showed how just the perfect fit was enough to increase the stress value of about 60 MPa. In the real condition of forced coupling (about 25 μm interference) the stress increase would be higher.
Stress map Fig. 16 shows how the maximum stress is reached on the outer edge of the case assy.
A parametrical simulation was carried out increasing the gap between the actuator case and the cap. Results showed that the stress became null at about 50 μm of gap (Fig. 17).

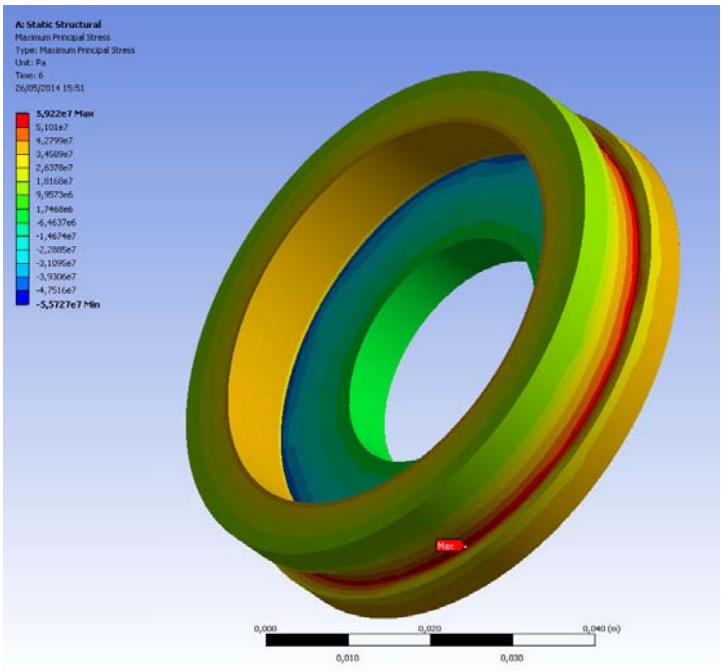

Figure 16: Stress Map.

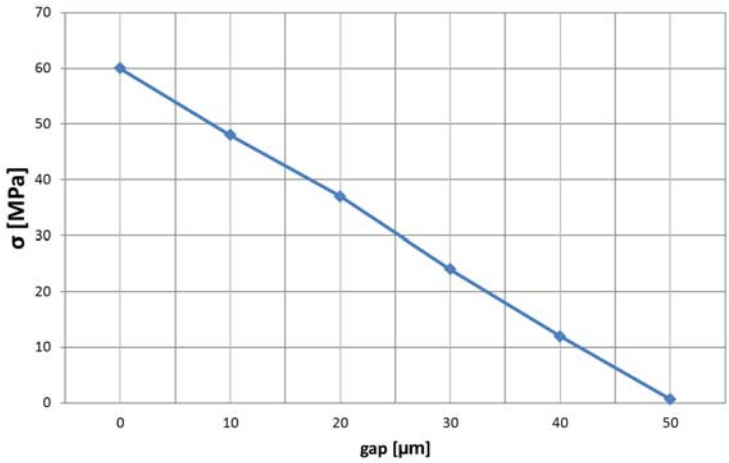

Figure 17: Transition between two halves of the actuator case.

Discussion

The examination of fracture surface showed a multisite fatigue phenomenon started from the external edge of actuator case. Chemical analysis and hardness measurement indicated that no unusual features were found in the material and his heat treatment. Metrological checks showed interference between the cap and the actuator case. The gap between the actuator and the cap has to be between 25.4 and 101.6 µm as design requirements. Tolerance between cap and actuator case is established taking in account thermal expansion. FEM analysis showed that less than 50 µm of gap between the two parts would induce abnormal stresses on the outer edge of the case assy due to the normal thermal conditions. These, in addition to the other normal operative loads, such as the actuation pressure, started the multiple initiation site fatigue

The evaluation of striations spacing features an high-cycle fatigue, compatible with vibration during flight [8] [3].

Conclusions

The Dual Booster Actuator failed because of a high-cycle multiple initiation sites fatigue mechanism. This was due to stress intensification caused by dimensional non conformances. Recommendations were issued in order to improve dimensional controls.

References

[1] Oddone, G., Guida alle interpretazioni delle caratteristiche morfologiche delle superfici di frattura al microscopio elettronico a scansione, Ragno Editore, (1981).
[2] Amura, M., Allegrucci, L., De Paolis, F., Bernabei, M., Fatigue fracture of an AMX aircraft main weel, Engineering Failure Analysis, 27 (2012)194-202.
[3] Cameron, D., Fatigue properties in engineering. Fatigue and fracture., ASM Handbook, (1996).
[4] Handbook, Metallography and Microstructure, George F. Vander Voort, 9 (2004).
[5] Handbook, Properties and Selection - Nonferrous Alloys and Special-Purpose Materials, (1990).
[6] MatWeb, www.MatWeb.com (2014).
[7] Taylor, R., Zienkiewicz, O.C., The Finite Element Method, 5th Ed., 2 (2000).
[8] Gugliotta, A., Introduzione alla meccanica della frattura lineare elastica., Levrotto & Bella, (2002).